Theoretical and Simulation-based Analysis of Terrestrial Interference to LEO Satellite Uplinks

Anastasia Yastrebova[1], Ilari Angervuori[2], Niloofar Okati[3], Mikko Vehkaperä[1], Marko Höyhtyä[1], Risto Wichman[2], and Taneli Riihonen[3]

[1]VTT Technical Research Centre of Finland, Oulu, Finland
e-mail: {anastasia.yastrebova, mikko.vehkapera, marko.hoyhtya}@vtt.fi
[2]Aalto University School of Electrical Engineering, Helsinki, Finland
e-mail: {ilari.angervuori, risto.wichman}@aalto.fi
[3]Faculty of Information Technology and Communication Sciences, Tampere University, Finland
e-mail: {niloofar.okati, taneli.riihonen}@tuni.fi

***Abstract*—The integration of satellite–terrestrial networks is beneficial in terms of the increase of the network capacity and coverage. In such a heterogeneous network, highly efficient spectrum utilization is extremely important. This could be achieved by the single frequency reuse which allows increasing the capacity at the cost of increased interference. Interference is one of the main parameters that limits the link-level performance in such a network. In this paper, we examine the frequency reuse scenario by analyzing the impact of terrestrial interference to the uplink of a low Earth orbiting (LEO) satellite constellation in the high International Mobile Telecommunications (IMT) frequency bands. To this end, we propose a novel stochastic geometry based analytical framework that is able to accommodate various aspects of realistic satellite networks. The accuracy of the analysis is verified by using advanced simulation tools.**

I. Introduction

The rapid proliferation of smart devices has lead to a tremendous increase in data traffic worldwide. To address the challenge of ever-growing network capacity demand, a combination of terrestrial networks and low Earth orbit (LEO) mega-constellations is envisioned to provide a high-throughput low-latency broadband connectivity everywhere [1], [2]. However, one critical question for the satellite–terrestrial network coexistence is how the scarce spectrum resources between the two systems are shared [3]–[5]. Aggressive frequency re-use maximizes the spectral usage but leads to increased interference and degradation in the link quality. Accurate prediction of the interference between the systems is therefore of great practical importance.

In the literature, the coexistence and spectrum sharing between the satellite and terrestrial systems has been studied extensively either through computer simulations or mathematical analysis [4], [6]–[10]. The problem of simulations is that they are time-consuming and require specialized software to be used. A similar problem is also encountered in terrestrial networks, where it has been solved successfully through the use of stochastic geometry; see for example [11]–[13] and references therein for an overview. However, examples of using stochastic geometry in satellite networks are very few. In [14], the interference caused by the terrestrial network to downlink transmission of a multibeam satellite on a geostationary orbit is investigated. The scenario is extended to a cognitive satellite–terrestrial system where the cellular network acts as the secondary user by the same authors in [15]. A general expression for a single LEO satellite's visibility time is provided in [16], but it is incapable of concluding the general distribution of visibility periods for any arbitrarily positioned user. The deterministic model in [16] was then developed by a statistical analysis of coverage time in mobile LEO during a satellite visit [17]. Very recently, stochastic geometry was used to study various aspects of LEO satellite systems with large constellations in the downlink direction [18], [19].

In this paper, stochastic geometry is applied for the performance analysis of integrated satellite–terrestrial systems in the uplink (UL) direction. In our model, the interfering terrestrial transmitters are randomly distributed according to the Poisson point process. As the distance to the horizon is limited, a satellite can only experience interference from a bounded area, which precludes the use of standard stochastic geometry analysis (as presented, e.g., in [20]), as this often involves an infinite domain. Given satellite constellation is modeled with an appropriate point process which will allow us to perform the theoretical analysis for the LEO constellations.

To the best of our knowledge, this is the first paper that considers the stochastic geometry based analysis of the UL scenario in LEO systems. In contrast to prior works, we also verify the results of stochastic geometry using the industry standard simulator developed by AGI, namely Systems Tool Kit (STK) [21]. This leads to realistic measurements via the accurate physics-based satellite propagation model, path loss models, etc. provided by the STK. In addition, through STK simulations we are able to examine the time evolution of the system as the satellites propagate over the area of interest.

The organization of the remainder of this paper is as follows. Section II describes the uplink scenario for a LEO constellation. As for the main results, in Section III, we derive analytical expressions for coverage probability. Verification of numerical results is provided in Section IV using STK. Finally, we conclude the paper in Section V.

II. System Model

Let us consider an uplink LEO communication satellite network, as shown in Fig. 1, in which the ground terminals can transmit data to a satellite if they are located within the footprint of satellite's coverage area. The satellite constellation consists of N satellites, which are placed on N_{o} low circular orbits with the same inclination angle and altitude denoted by ι and h, respectively. On each orbit, N_{q} satellites are distributed uniformly, i.e., $N = N_{\mathrm{o}} N_{\mathrm{q}}$.

Ground terminals are located on the surface of Earth which is approximated as a perfect sphere with radius $r_{\mathrm{E}} \approx 6371$ km. The serving ground terminal transmits the data to the nearest satellite while other terminals within the coverage footprint of the satellite cause interference. The interfering ground terminals belong to either the satellite network (SN) or the terrestrial network (TN). Different power levels are set for serving and interfering transmitted signals, denoted by p_0 and p_n, respectively.

For our analysis, we consider that the ground terminals, tagged as x_n, $n = 0, 1, \ldots, N-1$, are distributed according to a homogeneous Poisson point process Φ of intensity λ_{gt}, i.e., $x_n \in \Phi$. The distances from the transmitters to the satellite and their corresponding Earth-centered angles are denoted by R_n and γ_n, respectively. Throughout this paper, superscript zero always associates the parameter with the serving transmitter while other subscripts, $n \neq 0$, are reserved for interfering transmitters. As for the propagation model, we consider the mean power attenuation model given in [22] as well as Rician fading.

The ground terminals and satellites are equipped with omni-directional antennas with antenna gains of G_{gt} and G_{sat}, respectively. The satellite-centered angle between the center of Earth and the ground transmitter, θ, can be obtained from the basic geometry as

$$\theta(\gamma_n) = \frac{\pi}{2} - \gamma_n - \arcsin\left(\frac{\cos(\gamma_n)(r_{\mathrm{E}} + h) - r_{\mathrm{E}}}{R_n(\gamma_n)}\right),$$

where γ_n is the Earth-centered angle between the transmitter and the satellite as depicted in Fig. 1, and

$$R_n(\gamma_n) = \sqrt{\left(\cos(\gamma_n)(r_{\mathrm{E}} + h) - r_{\mathrm{E}}\right)^2 + \left(\sin(\gamma_n)(r_{\mathrm{E}} + h)\right)^2}. \quad (1)$$

Thus, path loss is a function of the radial distance γ_n and given by [22]

$$g(\gamma_n) = \frac{G(\theta(\gamma_n))}{R_n^{\alpha}(\gamma_n)}, \quad (2)$$

where α is the path loss exponent and $G = G_{\mathrm{sat}} G_{\mathrm{gt}}$.

Based on the above modeling, the signal-to-interference ratio (SIR) at the receiver satellite can be expressed as

$$\mathrm{SIR} = \frac{p_{\mathrm{v}_0}\, g(\gamma_0)}{I} = \frac{p_{\mathrm{v}_0}\, g(\gamma_0)}{\sum\limits_{x_n \in \Phi / x_0} p_{\mathrm{v}_n}\, g(\gamma_n)}, \quad (3)$$

where I is the cumulative interference power from all other transmitters than the serving transmitter, p_{v_0} and p_{v_n} indicate the virtual transmitted power from the serving and the interfering satellites, respectively. Based on our assumption regarding the Rician fading model, the virtual power is given by

$$p_{\mathrm{v}_0} = p_0 q + (1-q) p_0', \quad (4)$$

$$p_{\mathrm{v}_n} = p_n q + (1-q) p_n', \quad (5)$$

where p_0' and p_n' are exponential with mean p_0 and p_n, respectively, and $q \in [0, 1]$ represents the portion of line-of-sight component in the received signal.

Fading conditions of interfering transmitters are considered to be identically and independently distributed, and spectral efficiency is calculated by averaging over different channel realizations. The interference can be seen as Gaussian noise, and Shannon formula $C = \log_2(1 + \mathrm{SIR})$ can be used to measure the link capacity [23].

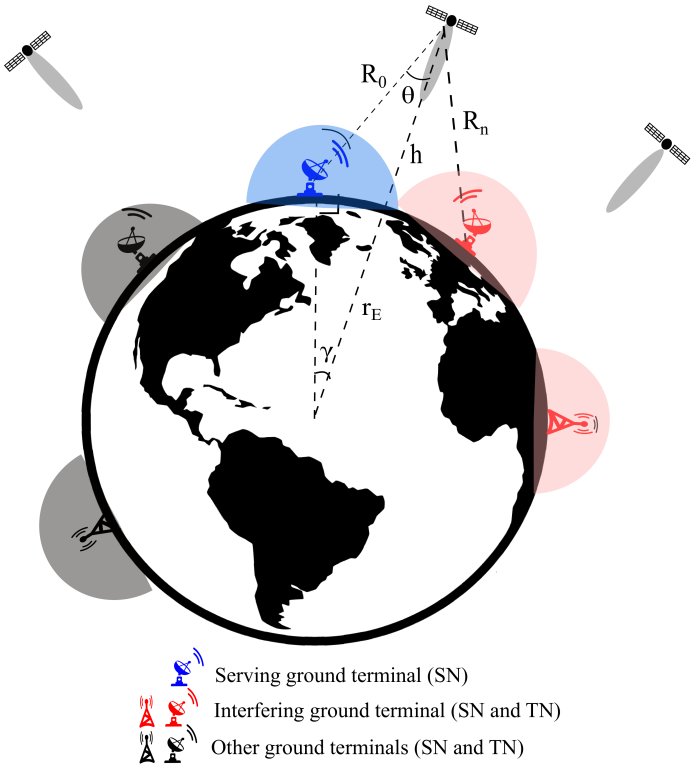

Fig. 1. Illustration of the considered uplink satellite network. The serving ground terminal transmits to its nearest satellite, while other ground terminals consist of satellite ground stations and terrestrial base stations may cause interference.

III. Theoretical Analysis

In this section, we provide the theoretical expression for the probability of coverage to the nearest satellite when the satellites are assumed to be distributed according to a Poisson point process with intensity λ_{sat}. The value for λ_{sat} is chosen so that it corresponds to the average density of satellites in a real constellation. This depends on the user location on Earth.

The theory is facilitated by the shot-noise theory of marked Poisson point processes and we refer to [20] for further information.

Proposition 1. *The uplink probability of coverage when satellites are distributed according to a Poisson point process with intensity λ_{sat} is*

$$p_c(T) = 2\pi\lambda_{sat}\int_0^{\beta}\int_{qp_0}^{\infty} F_I\left(\frac{p_{\text{v}_0}g(\gamma_0)}{T}\right)\frac{e^{-\frac{p_{\text{v}_0}-p_0q}{p_0(1-q)}}}{p_0(1-q)} \cdot \gamma_0 e^{-\lambda_{sat}\pi\gamma_0^2}dp_{\text{v}_0}d\gamma_0, \quad (6)$$

where T is the SIR threshold for a successful transmission and β refers to radial distance to a satellite at horizon which can be simply obtained from basic geometry as $\beta = \cos^{-1}\left(\frac{r_E}{r_E+h}\right)$.

Proof. To obtain (6), we start with the definition of coverage probability:

$$\begin{aligned}
&\mathbb{E}_{\gamma_0}\left[\mathbb{P}\left(\text{SIR} > T|\gamma_0\right)\right)] \\
&= \int_0^{\beta}\mathbb{P}\left(\text{SIR} > T|\gamma_0\right))\, f_{\gamma_0}(\gamma_0)d\gamma_0 \\
&\overset{(a)}{=} 2\pi\lambda_{\text{sat}}\int_0^{\beta}\mathbb{P}\left(\frac{p_{\text{v}_0}g(\gamma_0)}{I} \geq T\right)\gamma_0 e^{-\lambda_{\text{sat}}\pi\gamma_0^2}d\gamma_0 \\
&= 2\pi\lambda_{\text{sat}}\int_0^{\beta}\mathbb{E}_{p_{\text{v}_0}}\left[\mathbb{P}\left(I \leq \frac{p_{\text{v}_0}g(\gamma_0)}{T}|p_{\text{v}_0} > 0\right)\right] \\
&\qquad \cdot \gamma_0 e^{-\lambda_{\text{sat}}\pi\gamma_0^2}d\gamma_0 \\
&\overset{(b)}{=} 2\pi\lambda_{\text{sat}}\int_0^{\beta}\int_{qp_0}^{\infty} F_I\left(\frac{p_{\text{v}_0}g(\gamma_0)}{T}\right)\frac{e^{-\frac{p_{\text{v}_0}-p_0q}{p_0(1-q)}}}{p_0(1-q)} \\
&\qquad \cdot \gamma_0 e^{-\lambda_{\text{sat}}\pi\gamma_0^2}dp_{\text{v}_0}d\gamma_0. \quad (7)
\end{aligned}$$

Equation (a) follows from the substitution of the probability density function of γ_0 when satellites are distributed as a Poisson point process, i.e., $f_{\gamma_0}(\gamma_0) = 2\pi\lambda_{\text{sat}}\gamma_0 e^{-\lambda_{\text{sat}}\pi\gamma_0^2}$. Equation (b) is obtained by taking the expectation over the random variable p_{v_0}. Assuming that p_0' is exponential with mean p_0, the distribution can be simply obtained as $f_{p_{\text{v}_0}}(p_{\text{v}_0}) = \frac{e^{-\frac{p_{\text{v}_0}-p_0q}{p_0(1-q)}}}{p_0(1-q)}$. □

In the case of constant transmitting power, i.e., $q = 1$, we have simply

$$p_c(T) = 2\pi\lambda_{\text{sat}}\int_0^{\beta} F_I\left(\frac{p_0g(\gamma_0)}{T}\right)\gamma_0 e^{-\lambda_{\text{sat}}\pi\gamma_0^2}d\gamma_0. \quad (8)$$

Proposition 2. *The cumulative distribution function $F_I(t)$ in Proposition 1 is given by*

$$F_I(t) = 1 - \frac{2e^{at}}{\pi}\int_0^{\infty}\Re\left\{\frac{1-\mathcal{L}_I(a+iu)}{a+iu}\right\}\cos(ut)du. \quad (9)$$

Proof. Proposition (2) is derived using Broomwhich inverse contour integral and the property of the Laplace transform, $\mathcal{L}_X(s) := \mathbb{E}[e^{-sX}]$, which states that the Laplace transform of the CDF can be obtained from Laplace transform of the PDF by dividing by s in the frequency domain. Thus, we have

$$\begin{aligned}
1 - F_I(t) &= \frac{1}{2\pi i}\int_{a-i\infty}^{a+i\infty}\frac{1-\mathcal{L}_I(s)}{s}e^{st}ds \\
&= \frac{1}{2\pi}\int_{-\infty}^{\infty}\frac{1-\mathcal{L}_I(a+iu)}{a+iu}e^{(a+iu)t}du \\
&= \frac{e^{at}}{2\pi}\int_{-\infty}^{\infty}\frac{1-\mathcal{L}_I(a+iu)}{a+iu}(\cos(ut)+i\sin(ut))du \\
&= \frac{e^{at}}{2\pi}\int_{-\infty}^{\infty}\Re\left\{\frac{1-\mathcal{L}_I(a+iu)}{a+iu}\right\}\cos(ut) \\
&\qquad - \Im\left\{\frac{1-\mathcal{L}_I(a+iu)}{a+iu}\right\}\sin(ut)du \\
&\overset{(a)}{=} \frac{2e^{at}}{\pi}\int_0^{\infty}\Re\left\{\frac{1-\mathcal{L}_I(a+iu)}{a+iu}\right\}\cos(ut)du, \quad (10)
\end{aligned}$$

where $\Re\{\cdot\}$ and $\Im\{\cdot\}$ denote the real and imaginary parts of the complex arguments, respectively. Equation (a) follows from properties of real and imaginary parts in Laplace transform. Namely, for non-negatively supported $\hat{f}$:

$$\begin{aligned}
&\Re\{\hat{f}(a+iu)\}\cos(ut) - \Im\{\hat{f}(a+iu)\}\sin(ut) \\
&= 2\Re\{\hat{f}(a+iu)\}. \quad (11)
\end{aligned}$$

□

Proposition 3. *Laplace transform of the interference from Poisson distributed transmitters is given by*

$$\mathcal{L}_I(s) = \exp\left\{-2\pi\lambda_{gt}\int_0^{\beta}\gamma_n\big(1-\mathcal{L}_{p_{\text{v}_n}}(sg(\gamma_n))\big)d\gamma_n\right\}, \quad (12)$$

where

$$\begin{aligned}
\mathcal{L}_{p_{\text{v}_n}}(s) &= \mathcal{L}_{p_nq}(s)\mathcal{L}_{(1-q)p_n'}(s) \\
&= \exp\left(-p_nqs\right)\cdot\frac{1/p_n}{1/p_n+(1-q)s}. \quad (13)
\end{aligned}$$

Proof. Poisson point process in a bounded window $B := B(0,\beta) \subset \mathbb{R}^d$ conditioned on having n points in the window follows a binomial distribution. Furthermore, having n points inside the window B is Poisson distributed in Poisson p.p.

$$\mathbb{P}\{n \text{ points in } B\} = e^{-\lambda_{\text{gt}}\mathcal{V}(B)}\frac{(\lambda_{\text{gt}}\mathcal{V}(B))^n}{n!}, \quad (14)$$

where $\mathcal{V}(B)$ is the Lebesgue volume of B. Let $\gamma_1, \gamma_2, \ldots, \gamma_N$ be the distances of the points $x_1, x_2, \ldots, x_N \in \Phi$ from the origin and $p_{\text{v}_1}, p_{\text{v}_2}, \ldots, p_{\text{v}_N}$ the transmitting powers of the

respective points. From the definition of Laplace transform, we have

$$\begin{aligned}
\mathcal{L}_I(s) &= \mathbb{E}[e^{-sI}] = \mathbb{E}_{p_{\mathrm{v}_n},\gamma_n}\left[e^{-s\sum\limits_{x_n\in\Phi/x_0} p_{\mathrm{v}_n}\, g(\gamma_n)}\right] \\
&= \mathbb{E}_{p_{\mathrm{v}_n},\gamma_n}\left[e^{-\lambda_{\mathrm{gt}}\mathcal{V}(B)}\sum_{N=0}^{\infty}\frac{(\lambda_{\mathrm{gt}}\mathcal{V}(B))^N}{N!}e^{-s\sum\limits_{n=1}^{N} p_{\mathrm{v}_n}\, g(\gamma_n)}\right] \\
&= e^{-\lambda_{\mathrm{gt}}\mathcal{V}(B)}\sum_{N=0}^{\infty}\frac{(\lambda_{\mathrm{gt}}\mathcal{V}(B))^N}{N!} \\
&\quad\cdot \mathbb{E}_{p_{1,\ldots,n},\gamma_{1,\ldots,n}}\left[e^{-s\sum\limits_{n=1}^{N} p_{\mathrm{v}_n}\, g(\gamma_n)}\right] \\
&= e^{-\lambda_{\mathrm{gt}}\mathcal{V}(B)}\sum_{N=0}^{\infty}\frac{(\lambda_{\mathrm{gt}}\mathcal{V}(B))^N}{N!} \\
&\quad\cdot \mathbb{E}_{p_{\mathrm{v}_1},\gamma_1}\left[e^{-sp_{\mathrm{v}_1}\, g(\gamma_1)}\right]\cdot\ldots\cdot\mathbb{E}_{p_{\mathrm{v}_N},\gamma_N}\left[e^{-sp_{\mathrm{v}_N}\, g(\gamma_n)}\right] \\
&= e^{-\lambda_{\mathrm{gt}}\mathcal{V}(B)}\sum_{N=0}^{\infty}\frac{(\lambda_{\mathrm{gt}}\mathcal{V}(B))^N}{N!} \\
&\quad\cdot \frac{2\pi}{\mathcal{V}(B)^N}\left(\int_0^{\beta}\int_0^{\infty}\gamma e^{-sp_{\mathrm{v}_n}g(\gamma_n)}F(dp_{\mathrm{v}_n})d\gamma_n\right)^N \\
&\overset{(a)}{=} e^{-\int_0^{\beta}(1-\int_0^{\infty}e^{-sp_{\mathrm{v}_n}g(\gamma_n)}F(dp_{\mathrm{v}_n}))\lambda_{gt}d\gamma_n},
\end{aligned}$$

where measure F corresponds to the distribution of the power affected by the fading of the transmitters (virtual power). Equation (a) stems from series expansion of the exponential function. Equation (13) follows straightforwardly from the definition of p_{v_n} in (5) and from standard properties of Laplace transform. □

Point-wise values $F_I(t)$ in (9) can be numerically calculated through the Euler methods described in [24]. The following approximation

$$\begin{aligned}
F_I(t) = 1 &- \sum_{k=0}^{m}\binom{m}{k}2^{-m}\frac{e^{A/2}}{2t}\Re\left\{\frac{1-\mathcal{L}_I(A/2t)}{A/2t}\right\} \\
&+ \frac{e^{A/2}}{t}\sum_{k=1}^{n}(-1)^k\Re\left\{\frac{1-\mathcal{L}_I(\frac{A+2k\pi i}{2t})}{\frac{A+2k\pi i}{2t}}\right\} \qquad (15)
\end{aligned}$$

with $A = 18.4, m = 11$ and $n = 15$ is suggested here. The approximation is derived from applying trapezoidal method to (9) and improving the accuracy by Euler summation.

IV. Numerical Results

The analyzed scenario was implemented in the simulation environment STK and is depicted in Fig. 2. The system parameters for the simulations are summarized in Table I. The satellite altitude was chosen to be 550 km to partly investigate the performance of emerging very low Earth-orbiting satellite constellations, such as Starlink [25]. The simulated satellite constellation consists of 126 satellites, constructed according to the Walker method [26]. The minimum elevation angle for the ground terminals was chosen to be 10 degrees to allow satellite connectivity also in the presence of large obstacles such as buildings [27]. In the simulated scenario, 1676 interfering terminals were distributed randomly across the area of interest. The serving ground terminals were placed inside the area of interest in a way that they were surrounded by the interference sources. The analysis was performed over the 12-hour time period from 30 Apr 2020 09:00 to 30 Apr 2020 21:00. As explained in Section II, during this period the serving ground terminal always connects to the closest satellite it can find while other terminals act as interference sources.

Fig. 3 depicts the evolution of the signal-to-interference ratio (SIR) over time in the STK simulations. The spikes represent connections to new satellites and the blue dots represent the ongoing connections with a time step of 10 seconds. The closer the satellite is to the serving ground terminal, the higher the SIR and the better the signal quality is. The aim of the simulations was to investigate the frequency

TABLE I
System parameters

Satellite constellation parameters	
Altitude (h) [km]	550
Number of satellite orbits (N_{o})	9
Number of satellites per orbit (N_{q})	14
Inclination of the orbits (ι)	90°
Ground terminal parameters	
Carrier frequency f [GHz]	26
Power of serving transmitter p_0 [dBW]	-6
Serving transmitter antenna gain [dB]	37
Serving transmitter antenna model	ITU-R S.465
Power of interfering transmitters p_n [dBW]	varying
Number of interfering terminals	1676
Interference antenna model	Isotropic
Satellite antenna model	Isotropic
SIR threshold for successful decoding T [dB]	10

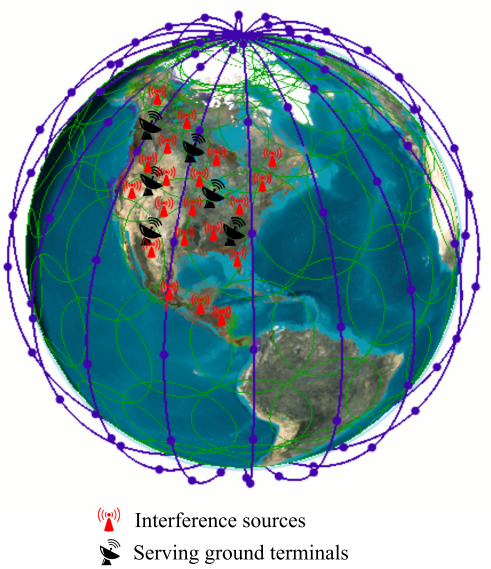

Fig. 2. STK scenario representing used satellite constellation, interference sources, and serving ground terminals. Green circles represent the satellite footprint.

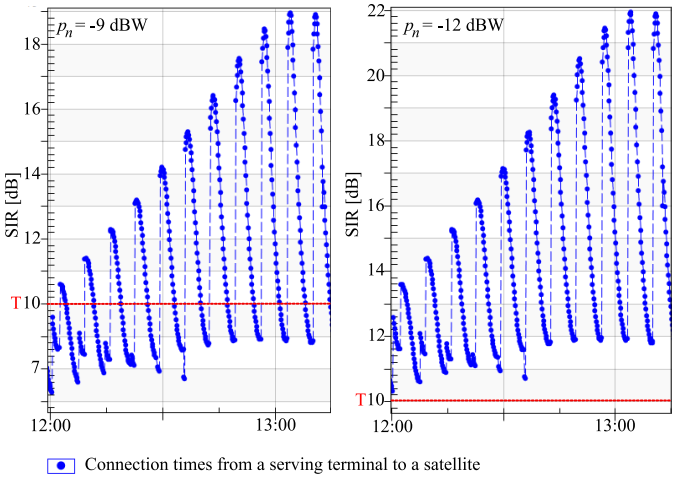

Fig. 3. Time evolution of SIR for serving ground terminal for interference powers $p_n = -9$ dBW and $p_n = -12$ dBW. The blue dots represent the connection times to a satellite with the time step 10 sec. Line-of-sight channel was assumed between the serving ground terminal and the satellite. The threshold (T) for successful decoding is $T = 10$ dB.

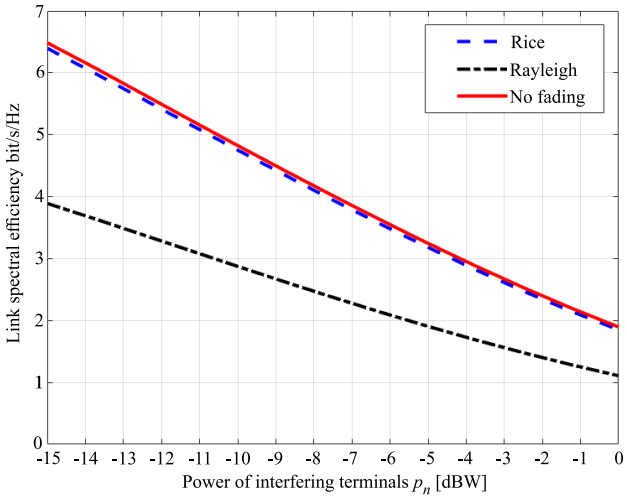

Fig. 4. Spectral efficiency $\mathbb{E}[\log_2(1 + \text{SIR})]$ bit/s/Hz of the satellite uplink. Values were acquired by the analysis. Approximately mean 1010 interfering transmitters were assumed to be located inside the satellite footprint. Interfering terminals were assumed to have LoS channel while the serving ground terminal experienced Rayleigh, Rician (with K factor $K = 10$) or LoS fading channels.

reuse performance in the satellite–terrestrial network in a high IMT frequency band, specifically how much the desired link from serving terminals is affected by the interference sources with varying powers. In the considered line-of-sight (LoS) condition, the SIR drops below the chosen decoding threshold $T = 10$ dB multiple times during the considered time period when the power of interfering transmitters is $p_n = -9$ dBW. The probability of successful decoding, or probability of coverage $p_c(T)$, during the entire 12-hour period was around 0.48 in the scenario considered in Fig. 3, implying unacceptable quality of the desired link. When the power of the interfering transmitters was reduced to $p_n = -12$ dBW, the

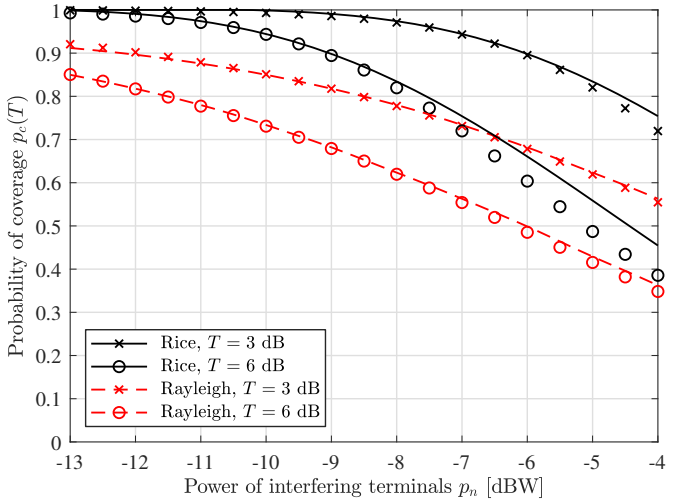

Fig. 5. Coverage probability as a function of the power of interfering sources. Markers depict the STK simulations and the lines correspond to the analytical results. Interfering terminals were assumed to have LoS channels while the serving ground terminal experienced Rayleigh or Rician fading (with K factor $K = 10$) channels.

SIR was above the threshold during the entire depicted period and the probability of coverage for the 12-hour simulation period was $p_c(T) \approx 0.89$. According to the simulation results, the interference power that is lower than -11 dBW provides desired link quality with coverage probability of at least $p_c(T) = 0.80$.

While STK simulations provide accurate results and enable investigation of the time evolution of the system, they require specialized software and are computationally complex for the studied scenario that has multiple simultaneous interfering transmissions. The simulation execution time on the HP EliteBook 840 G5 laptop with the current scenario settings reaches 30 minutes per iteration. The analytical results provided in Section III, on the other hand, provide a very fast method for examining the performance of the system with different parameter values. Fig. 4 represents analytically examined spectral efficiency of the satellite uplink. In the calculations, interfering transmitters were assumed to be located inside the satellite footprint with LoS channel, while the serving ground terminal experienced Rayleigh, Rician (with K factor $K = 10$) or LoS fading channels.

To verify the accuracy of the analysis, Fig. 5 presents the STK simulation results and the corresponding results from the analytical framework described in Section III. In the figure, the STK simulations are depicted with markers and the lines correspond to the analytical results. In this scenario, the interfering terminals have LoS to the satellite, while the serving ground terminal is assumed to experience Rayleigh or Ricean fading with K factor $K = 10$.

Since the STK framework used in this paper did not support direct simulation of fast fading channels, the simulations were carried out in two phases. First, the long term channel effects were simulated with STK and exported as text files. Second,

fast fading was added to the long term channel conditions using Matlab and the final SIR calculations were carried out. It should also be noted that the simplified Rician fading model used in the analysis is only an approximation of the true Rician fading used in the simulations. Herein the parameter q was selected so that the probability density of the channel powers had equal first and second moments. This was achieved by selecting $q = 1 - \sqrt{\frac{1+2K}{(K+1)^2}}$.

The simulations and analysis have a good match in all considered cases when the interference power is low, or the coverage probability satisfies $p_c(T) > 0.85$. With Rayleigh fading in the desired link, the analysis follows the simulations closely also when the coverage probability is much lower. The result implies that the analytical framework proposed in this paper is useful for predicting the performance of real satellite systems in the region of coverage probabilities that is of practical interest. Furthermore, the result shows that if the desired link experiences fading, the interference tolerance is significantly reduced compared to the LoS case considered in Fig. 3.

V. Conclusion

In this paper, we presented a mathematical framework for uplink coverage analysis of a terrestrial–satellite network using stochastic geometry. The satellite network is, first, modeled with a Poisson point process which was then utilized to obtain exact expressions for coverage probability in terms of network parameters. Using Systems Tool Kit simulations, we verified the correctness of our derivations. The analytical results provided in this paper can make a huge impact on the development and design of dense satellite networks. Regarding the impact of terrestrial interference to the satellite uplink, current simulations have shown that without a suitable configuration the level of the interference to the uplink can lead to unacceptable performance. Strict power limits for the transmission in the shared bands or mechanisms such as licensed shared access are required to limit the number of simultaneously accessing users in the band.

Acknowledgment

The work of N. Okati and T. Riihonen was supported by a Nokia University Donation. The work of M. Vehkaperä was supported by the PRIORITY project, partly funded by Business Finland.

References

[1] J. Liu, Y. Shi, Z. M. Fadlullah, and N. Kato, "Space-air-ground integrated network: A survey," *IEEE Communications Surveys & Tutorials*, vol. 20, no. 4, pp. 2714–2741, 2018.

[2] P. Wang, J. Zhang, X. Zhang, Z. Yan, B. G. Evans, and W. Wang, "Convergence of satellite and terrestrial networks: A comprehensive survey," *IEEE Access*, vol. 8, pp. 5550–5588, 2020.

[3] ETSI, "ETSI TR 103 124 V1.1.1, Satellite Earth Stations and Systems (SES); Combined Satellite and Terrestrial Networks scenarios," European Telecommunications Standards Institute, Tech. Rep., 2013.

[4] J. Ylitalo, A. Hulkkonen, M. Höyhtyä, A. Byman, M. Leinonen, J. Janhunen, and A. Roivainen, "Hybrid satellite systems: Extending terrestrial networks using satellites," in *Cooperative and Cognitive Satellite Systems*. Elsevier, 2015, pp. 337–371.

[5] M. Höyhtyä, A. Hekkala, M. D. Katz, and A. Mämmelä, "Spectrum awareness: techniques and challenges for active spectrum sensing," in *Cognitive wireless networks*. Springer, 2007, pp. 353–372.

[6] Z. Qu, Z. Liu, X. Ding, H. Cao, and G. Zhang, "Co-existence analysis on satellite-terrestrial integrated IMT system," *Mobile Networks and Applications*, vol. 24, no. 6, pp. 1926–1936, 2019.

[7] J. Janhunen, J. Ketonen, A. Hulkkonen, J. Ylitalo, A. Roivainen, and M. Juntti, "Satellite uplink transmission with terrestrial network interference," in *2015 IEEE global communications conference (GLOBECOM)*. IEEE, 2015, pp. 1–6.

[8] E. Lagunas, S. Maleki, L. Lei, C. Tsinos, S. Chatzinotas, and B. Ottersten, "Carrier allocation for hybrid satellite-terrestrial backhaul networks," in *2017 IEEE International Conference on Communications Workshops (ICC Workshops)*. IEEE, 2017, pp. 718–723.

[9] Y. Zhang, Y. Shi, F. Shen, Y. Pang, F. Yan, and L. Shen, "Satellite-terrestrial spectrum sensing scheme based on cascaded fnn and fis," in *2019 IEEE Globecom Workshops (GC Wkshps)*, 2019, pp. 1–6.

[10] X. Zhu, C. Jiang, W. Feng, L. Kuang, Z. Han, and J. Lu, "Resource allocation in spectrum-sharing cloud based integrated terrestrial-satellite network," in *2017 13th International Wireless Communications and Mobile Computing Conference (IWCMC)*, 2017, pp. 334–339.

[11] M. Haenggi, *Stochastic geometry for wireless networks*. Cambridge University Press, 2012.

[12] H. ElSawy, E. Hossain, and M. Haenggi, "Stochastic geometry for modeling, analysis, and design of multi-tier and cognitive cellular wireless networks: A survey," *IEEE Communications Surveys and Tutorials*, vol. 15, no. 3, pp. 996–1019, Jun. 2013.

[13] B. Błaszczyszyn, M. Haenggi, P. Keeler, and S. Mukherjee, *Stochastic geometry analysis of cellular networks*. Cambridge University Press, 2018.

[14] M. Sellathurai, S. Vuppala, and T. Ratnarajah, "User selection for multi-beam satellite channels: A stochastic geometry perspective," in *Proc. Asilomar Conference on Signals, Systems and Computers*, Nov. 2016.

[15] O. Y. Kolawole, S. Vuppala, M. Sellathurai, and T. Ratnarajah, "On the performance of cognitive satellite–terrestrial networks," *IEEE Transactions on Cognitive Communications and Networking*, vol. 3, no. 4, pp. 668–683, Dec. 2017.

[16] I. Ali, N. Al-Dhahir, and J. E. Hershey, "Predicting the visibility of LEO satellites," *IEEE Transactions on Aerospace and Electronic Systems*, vol. 35, no. 4, pp. 1183–1190, Oct. 1999.

[17] Y. Seyedi and S. M. Safavi, "On the analysis of random coverage time in mobile LEO satellite communications," *IEEE Communications Letters*, vol. 16, no. 5, pp. 612–615, May 2012.

[18] N. Okati, T. Riihonen, D. Korpi, I. Angervuori, and R. Wichman, "Downlink coverage and rate analysis of low Earth orbit satellite constellations using stochastic geometry," *IEEE Transactions on Communications*, vol. 68, no. 8, pp. 5120–5134, Aug. 2020.

[19] N. Okati and T. Riihonen, "Stochastic analysis of satellite broadband by mega-constellations with inclined LEOs," in *Proc. IEEE 31st Annual International Symposium on Personal, Indoor and Mobile Radio Communications (PIMRC)*, Sep. 2020.

[20] F. Baccelli and B. Błaszczyszyn, "Stochastic geometry and wireless networks, volume I—Theory, volume 3, no 3–4 of foundations and trends in networking," 2009.

[21] Analytical Graphics, Inc., "AGI's ready-to-use STK and ODTK families of products, enterprise software, and developer tools," [Online] https://www.agi.com/products, 2020.

[22] F. Baccelli, B. Błaszczyszyn *et al.*, "Stochastic geometry and wireless networks: Volume II applications," *Foundations and Trends® in Networking*, vol. 4, no. 1–2, pp. 1–312, 2010.

[23] P. V. Tse. D., *Fundamentals of Wireless Communication*. Cambridge University Press, 2005.

[24] Abate and W. Whitt, "Numerical inversion of Laplace transforms of probability distributions," *ORSA Journal on Computing*, vol. 7, no. 1, p. 36–43, 1995.

[25] Federal Communications Commission, "Application for modification of authorization for the SpaceX NGSO satellite system," [Online] https://fcc.report/IBFS/SAT-MOD-20190830-00087/1877764.pdf, 2019.

[26] A. Yastrebova, M. Höyhtyä, and M. Majanen, "Mega-constellations as enabler of autonomous shipping," in *2019 International Communications Satellite Systems Conference (ICSSC)*, Oct. 2019.

[27] O. L. De Weck, U. Scialom, and A. Siddiqi, "Optimal reconfiguration of satellite constellations with the auction algorithm," *Acta Astronautica*, vol. 62, no. 2-3, pp. 112–130, 2008.